

The Search for $\mu^+ \rightarrow e^+ \gamma$ with 10^{-14} Sensitivity: the Upgrade of the MEG Experiment

The MEG II Collaboration

Alessandro M. Baldini ^{1a} , Vladimir Baranov ², Michele Biasotti ^{3ab}, Gianluigi Boca ^{4ab} , Paolo W. Cattaneo ^{4a} , Gianluca Cavoto ^{5ab} , Fabrizio Cei ^{1ab} , Marco Chiappini ^{1ab} , Gianluigi Chiarello ^{5ab} , Alessandro Corvaglia ^{6ab} , Federica Cuna ^{6ab} , Giovanni dal Maso ^{1ab,9} , Antonio de Bari ^{4ab} , Matteo De Gerone ^{3a} , Marco Francesconi ^{1ab} , Luca Galli ^{1a} , Giovanni Gallucci ^{3a} , Flavio Gatti ^{3ab} , Francesco Grancagnolo ^{6a} , Marco Grassi ^{1a} , Dmitry N. Grigoriev ^{7,8}, Malte Hildebrandt ⁹ , Kei Ieki ¹⁰, Fedor Ignatov ⁷, Toshiyuki Iwamoto ¹⁰ , Peter-Raymond Kettle ⁹, Nikolay Khomutov ², Satoru Kobayashi ¹⁰ , Alexander Kolesnikov ², Nikolay Kravchuk ², Victor Krylov ², Nikolay Kuchinsky ², William Kyle ¹¹ , Terence Libeiro ¹¹, Vladimir Malyshev ², Manuel Meucci ^{5ab} , Satoshi Mihara ¹² , William Molzon ¹¹ , Toshinori Mori ¹⁰ , Alexander Mtchedlishvili ⁹, Mitsutaka Nakao ¹⁰, Donato Nicolò ^{1ab} , Hajime Nishiguchi ¹² , Shinji Ogawa ¹⁰, Rina Onda ¹⁰ , Wataru Ootani ¹⁰, Atsushi Oya ¹⁰, Dylan Palo ¹¹ , Marco Panareo ^{6ab} , Angela Papa ^{1ab,9} , Valerio Pettinacci ^{5a} , Alexander Popov ⁷, Francesco Renga ^{5a} , Stefan Ritt ⁹ , Massimo Rossella ^{4a} , Aleksander Rozhdestvensky ², Patrick Schwendimann ^{9,13}, Kohei Shimada ¹⁰, Giovanni Signorelli ^{1a} , Alexey Stoykov ⁹ , Giovanni F. Tassielli ^{6ab} , Kazuki Toyoda ¹⁰, Yusuke Uchiyama ^{10,*} , Masashi Usami ¹⁰, Cecilia Voena ^{5a,*} , Kosuke Yanai ¹⁰, Kensuke Yamamoto ¹⁰, Taku Yonemoto ¹⁰ and Yury V. Yudin ⁷

- 1 INFN Sezione di Pisa^a; Dipartimento di Fisica^b dell'Università, Largo B. Pontecorvo 3, 56127 Pisa, Italy
- 2 Joint Institute for Nuclear Research, 141980 Dubna, Russia
- 3 INFN Sezione di Genova^a; Dipartimento di Fisica^b dell'Università, Via Dodecaneso 33, 16146 Genoa, Italy
- 4 INFN Sezione di Pavia^a; Dipartimento di Fisica^b dell'Università, Via Bassi 6, 27100 Pavia, Italy
- 5 INFN Sezione di Roma^a; Dipartimento di Fisica^b dell'Università "Sapienza", Piazzale A. Moro 2, 00185 Rome, Italy
- 6 INFN Sezione di Lecce^a; Dipartimento di Matematica e Fisica^b dell'Università del Salento, Via per Arnesano, 73100 Lecce, Italy
- 7 Budker Institute of Nuclear Physics of Siberian Branch of Russian Academy of Sciences, 630090 Novosibirsk, Russia
- 8 Novosibirsk State Technical University, 630092 Novosibirsk, Russia
- 9 Paul Scherrer Institut PSI, 5232 Villigen, Switzerland
- 10 ICEPP, The University of Tokyo, 7-3-1 Hongo, Bunkyo-ku, Tokyo 113-0033, Japan
- 11 University of California, Irvine, CA 92697, USA
- 12 KEK, High Energy Accelerator Research Organization 1-1 Oho, Tsukuba, Ibaraki 305-0801, Japan
- 13 Swiss Federal Institute of Technology ETH, 8093 Zurich, Switzerland
- * Correspondence: cecilia.voena@roma1.infn.it; Tel.: +39-06-49914268 (C.V.), uchiyama@icepp.s.u-tokyo.ac.jp; Tel.: +81-3-3815-8384 (Y.U.)



Citation: Baldini, A. M.; Baranov, V.; Biasotti, M. et al. The Search for $\mu^+ \rightarrow e^+ \gamma$ with 10^{-14} Sensitivity: the Upgrade of the MEG Experiment. *Preprints* **2021**, *1*, 0. <https://doi.org/>

Received:
Accepted:
Published:

Publisher's Note: MDPI stays neutral with regard to jurisdictional claims in published maps and institutional affiliations.

Abstract: The MEG experiment took data at the Paul Scherrer Institute in the years 2009–2013 and published the most stringent limit on the charged lepton flavor violating decay $\mu^+ \rightarrow e^+ \gamma$: $\text{BR}(\mu^+ \rightarrow e^+ \gamma) < 4.2 \times 10^{-13}$ at 90% confidence level. The MEG detector has been upgraded in order to reach a sensitivity of 6×10^{-14} . The basic idea of MEG II is to achieve the highest possible sensitivity using the available muon beam intensity at the Paul Scherrer Institute (7×10^7 muons/s) with an improved detector. The key improvements are increased rate capability of all subsystems and increased resolutions while maintaining the same detector concept. In this paper, we present the current status of the preparation, integration and commissioning of the MEG II detector in the recent engineering runs.

Keywords: Lepton flavour violation; rare muon decay; high intensity experiment; particle detector; physics beyond the Standard Model

1. Introduction

Charged Lepton Flavor Violation (CLFV) processes are allowed in the Standard Model (SM) of elementary particle physics, accounting for measured neutrino mass differences and mixing angles, at extremely small branching ratios ($\ll 10^{-50}$). Since they are free of SM background, they are ideal probes for New Physics (NP) searches. CLFV transitions have been searched for in a variety of channels, but no evidence has been found so far. Nonetheless, they are predicted at measurable rates, not far from present experimental limits, by many SM extensions [1] and in particular in light of the recent muon $g - 2$ precision measurement [2] at Fermilab (see for example [3]).

Among the CLFV processes, the decay $\mu^+ \rightarrow e^+ \gamma$ is particularly sensitive to NP. The MEG experiment at the Paul Scherrer Institute (PSI) has searched for this decay in the period 2009–2013, and set the current best world limit to its branching ratio: $BR(\mu^+ \rightarrow e^+ \gamma) < 4.2 \times 10^{-13}$ at 90% confidence level [4].

Other CLFV channels actively pursued are $\mu^- N \rightarrow e^- N$, $\mu \rightarrow 3e$, $\tau \rightarrow \ell \gamma$ and $\tau \rightarrow \ell \ell \ell$ ($\ell = e, \mu$). The $\mu^- N \rightarrow e^- N$ conversion will be searched for by the DeeMe [5] and COMET [6] experiments in preparation at J-PARC. COMET will reach a sensitivity of $\mathcal{O}(10^{-15})$ in its first phase, to be compared with the existent limit of 7×10^{-13} [7] while in a second phase, it aims for a sensitivity of $\mathcal{O}(10^{-17})$. Another experiment, Mu2e [8] under construction at Fermilab, will search for $\mu^- N \rightarrow e^- N$ aiming to a sensitivity of 3×10^{-17} . The $\mu \rightarrow 3e$ search is being pursued in a new experiment currently in the commissioning phase at PSI: Mu3e [9], that in a staged approach plans to reach a sensitivity of 10^{-16} , to be compared with the existent limit of 1×10^{-12} [10]. CLFV decays involving τ leptons will be studied at the Belle II [11] experiment at Super KEKB with a sensitivity goal of $\mathcal{O}(10^{-9})$. Experiments at a super Charm-Tau factory [12], approved by the Russian government and presently in the R&D phase, were proposed with a sensitivity reach of the same order of magnitude. The sensitivity to NP in the different μ and τ channels is model dependent and all the above modes can be considered powerful probes to explore NP, complementary to direct searches at LHC and HL-LHC.

The MEG II experiment, under commissioning at the PSI, aims for a sensitivity enhancement compared to the MEG final result, $\mathcal{O}(6 \times 10^{-14})$. MEG II has the same experimental concept as MEG, that is discussed in the next section, but faces the challenge of a more intense muon beam with the need of keeping high efficiency and detector resolutions. The full MEG II proposal can be found in [13]. In this paper, we review the main aspects of the design and we report the results obtained in the engineering runs in the years 2017–2020, in view of the 2021 run that will be the first with the whole detector instrumented. An update of the expected sensitivity is also presented.

2. Experimental Components and Methods

2.1. The Experimental Approach

In $\mu^+ \rightarrow e^+ \gamma$ search experiments, positive muons are stopped in a thin target in order to exploit the very clear signature of a decay at rest: an e^+ and a γ in coincidence, moving collinearly back-to-back with their energies equal to half of the muon mass ($m_\mu/2 = 52.8$ MeV). The signal of the $\mu^+ \rightarrow e^+ \gamma$ decay can then be distinguished from the background by measuring the photon energy E_γ , the positron momentum p_{e^+} , their relative angle $\Theta_{e^+ \gamma}$ and timing $t_{e^+ \gamma}$ with the best possible resolutions.

The background comes either from radiative muon decays (RMD, $\mu^+ \rightarrow e^+ \nu \bar{\nu} \gamma$) in which the neutrinos carry away only a small amount of energy, or from an accidental coincidence of an energetic positron from Michel decay ($\mu^+ \rightarrow e^+ \nu \bar{\nu}$) with a photon coming from RMD, bremsstrahlung or positron annihilation-in-flight (AIF, $e^+ e^- \rightarrow \gamma \gamma$). Since the rate of accidental background events varies quadratically with the muon stopping rate, it cannot be

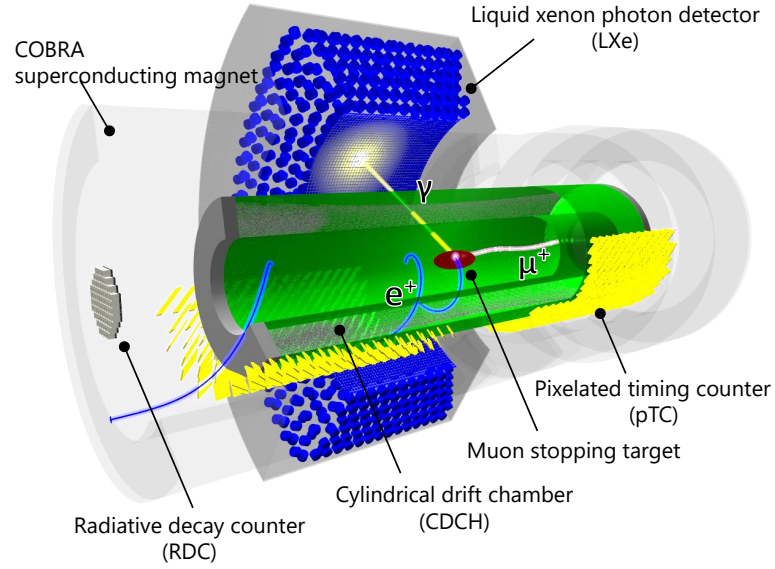


Figure 1. A schematic view of the MEG II experiment.

increased arbitrarily but must be chosen in order to limit the signal to background ratio and optimize the discovery potential.

The MEG II detector, shown schematically in Figure 1, is based on the same experimental concept as MEG and uses the same beam, but at the increased intensity of $7 \times 10^7 \mu^+/\text{s}$.

The positron spectrometer uses a gradient magnetic field and measures positron tracks with a newly designed low-mass single-volume cylindrical drift chamber (CDCH) able to sustain high rates. The positron time is measured with improved accuracy by a new pixelated timing counter (pTC). The acceptance of the spectrometer is increased by more than a factor two with respect to MEG. The photon is measured by an upgraded liquid xenon calorimeter (LXe) with a more uniform collection of scintillation light. This is achieved by replacing the MEG photomultiplier tubes (PMTs) on the photon entrance face with smaller vacuum-ultraviolet (VUV) sensitive silicon photomultipliers (SiPMs). A novel device for active suppression of the accidental background is introduced, the radiative decay counter (RDC). The trigger and data-acquisition system is also upgraded to meet the stringent requirements of an increased number of readout channels and to cope with the required bandwidth. Moreover, several auxiliary devices have been developed to monitor the beam and calibrate the detectors. The MEG II subsystems are described in the following subsections focusing on the changes from MEG, while the details of the MEG system can be found in [14].

2.2. The Muon Beam and the Target

Various combinations of beam momentum and target have been investigated to increase the muon stopping rate from $3 \times 10^7 \mu^+/\text{s}$ to $7 \times 10^7 \mu^+/\text{s}$ while preserving a low material budget along the beam line and in the target region. The configuration chosen is a surface muon beam of $28 \text{ MeV}/c$ (as in MEG) with a scintillating target of $140 \mu\text{m}$ thickness, placed at an angle of 15° with respect to the beam axis, which allows a simultaneous non-destructive beam intensity and profile measurement. A photogrammetric method to monitor the target position, orientation and shape has been implemented, thus addressing one of the dominant systematic effect in MEG. The system includes two CCD cameras and LEDs placed at one of the CDCH endplates, which optically monitor a printed patterns (dots) on the target [15][16].

Three new detectors have been developed to measure the beam profile and rate, to complement the well established methods used in MEG, i.e., a scanning pill-counter at the collimator and a scanning APD detector at the centre of the spectrometer. The first is a sampling scintillating fibre beam monitor, mounted at the entrance to the spectrometer. The second is a luminophore foil detector (CsI on a Mylar support) coupled with a CCD camera installed at the intermediate focus collimator system. The third one is a MatriX detector consisting of a 9×9 matrix of small scintillation counters, which is used at the centre of the spectrometer.

2.3. The Constant Bending Radius Magnet

The COBRA (COnstant Bending RAdius) solenoid, inherited from MEG, is a thin-walled, superconducting magnet with an axially graded magnetic field, ranging from 1.27 T at the centre to 0.49 T at either end of the magnet cryostat. The graded field has the advantage over a uniform solenoidal field such that particles produced with small longitudinal momentum have a much shorter latency time in the spectrometer, allowing stable operation in a high-rate environment. Additionally, the graded magnetic field is designed so that positrons emitted from the target follow a trajectory with almost constant projected bending radius, only weakly dependent on the emission polar angle. The COBRA magnet is equipped with a pair of compensation coils to reduce the stray field to the level necessary to operate the PMTs in the LXe detector.

2.4. The Detector

2.4.1. The Cylindrical Drift Chamber (CDCH)

The new MEG II positron tracker is a single volume drift chamber with cylindrical symmetry along the muon beam axis. The length is 191 cm and the radial extent ranges from 17 to 29 cm. The high granularity is ensured by nine layers of 192 drift cells, each a few mm wide. The wires form an angle with the CDCH axis, varying from 6° in the innermost layer to 8.5° in the outermost one. The stereo angle has an alternating sign, depending on the layer, allowing the longitudinal hit coordinate to be reconstructed. The single drift cell is quasi-square with a $20 \mu\text{m}$ Au-plated W sense-wire surrounded by 40 or $50 \mu\text{m}$ Ag-plated Al field wires, with a 5:1 field-to-sense wire ratio. The sensitive volume is filled with a low-mass He: iC_4H_{10} (90:10) gas mixture (plus some small quantities of additives to improve the operational stability), which is a good compromise between low scattering (radiation length $1.5 \times 10^{-3} X_0$) and single-hit resolution ($<120 \mu\text{m}$, measured on prototypes [17]).

Aluminum wire breaking problems arose during the CDCH assembly and commissioning, despite the fact that all the operations were performed inside clean rooms with a strict monitoring of the environmental conditions. The problem was deeply investigated by performing optical inspections with microscopes, chromatography, practical tests and SEM/EDS (Scanning Electron Microscopy with Energy Dispersive Spectroscopy) analyses. Chemical and mechanical analyses showed that the origin of the breaking phenomenon is the chemical corrosion of the Al core in presence of water condensation on wires from ambient humidity. Keeping the wire volume in an absolutely dry atmosphere with a continuous flow of inert gas (nitrogen or helium) proved to be effective in stopping the development of corrosion. The total number of broken cathode wires amounts to 97 (10) for diameters of 40 (50) μm . By simulating the drift cells electric field with Garfield [18] and ANSYS [19], the effect of a missing cathode wire on the reconstruction was found to be totally negligible.

The front-end electronic is constituted by custom boards, which also supply HV to the wires from one side and read out signals at both wire ends. The heat generated by the active electronics is cooled by a chiller system. The HV is supplied by a commercial HV [20] system

made of high precision modules, while a custom made gas system [21] flushes and monitors the gas mixture to the chamber and helium to COBRA.

2.4.2. The Pixelated Timing Counter (pTC)

The e^+ time must be precisely measured by the pTC with a resolution of about 40 ps, at a hit rate of 5 MHz. This is needed to allow for a precise measurement of the time coincidence of the $e^+\gamma$ pair. In addition, it also generates trigger signals by providing prompt timing and direction information on the e^+ . The pTC is composed of 512 scintillator counters. There are two sectors, placed on the upstream side and downstream side of the target, each consisting of 256 counters. The signal e^+ , curled by the COBRA magnetic field, hits on average 9 counters, significantly improving the total time resolution compared to MEG. The background hit rate on a single counter is suppressed to less than 100 kHz even though the beam intensity is twice as high as in MEG.

A single counter is composed of a fast plastic scintillator plate, BC-422 ($120 \times 40 \times 5 \text{ mm}^3$ or $120 \times 50 \times 5 \text{ mm}^3$ depending on the counter location) and six SiPMs connected in series at each end. The resolution of all assembled counters was measured with a ^{90}Sr source and found to be below 100 ps. The average resolution is 72 (81) ps for $120 \times 40(50) \times 5 \text{ mm}^3$ counters. The variations of the counter resolutions come from the variations of the photon detection efficiency amongst SiPMs and variations of the light yield between the scintillators.

The pTC is equipped with a cooling system to reduce dark count rates in the SiPMs [22] and a laser calibration system [23] to calibrate the timing between the counters.

2.4.3. The Liquid Xenon Calorimeter (LXe)

The liquid xenon detector is a key ingredient for identifying the signal and suppressing the background in the $\mu^+ \rightarrow e^+\gamma$ search, allowing the measurement of the photon's energy, time and position. The MEG LXe detector was one of the world's largest xenon based detectors with 900 L of liquid xenon. It was surrounded by 846 2-inch PMTs to detect the scintillation light emitted in the VUV range at a temperature of 165 K. Its performance was limited due to the non-uniform coverage of the PMT sensitive area, especially on the photon entrance face. While we reuse the liquid xenon and the cryostat in MEG II, we have upgraded it by replacing the PMTs on the photon entrance face with smaller photosensors, in order to reduce the non-uniformity of the detector response. In addition, the layout of the PMTs on the lateral faces was rearranged to improve light collection for events near the lateral walls. We inherited several methods to carefully calibrate the detector from MEG, with some modifications to match the upgraded configuration. The designed energy and position resolutions are $\sim 0.5 \text{ MeV}$ and $\sim 2.5 \text{ mm}$, respectively.

A new type of VUV sensitive SiPM, the VUV-MPPC [24], was developed. It is insensitive to magnetic fields and is sensitive to single photons, which enables an easier and more reliable calibration of the detector. Moreover, a finer readout granularity allows a more precise reconstruction of events where the initial high energy photons convert near the entrance face (shallow events) and to reduce pile-up of these photons in the same acquisition window. Thus, 216 PMTs at the entrance face are replaced by 4,092 SiPMs. A VUV-MPPC consists of four $6 \times 6 \text{ mm}^2$ sensor chips and the signals are read out by one channel per SiPM, connecting the four chips in series inside a PCB.

2.4.4. The Radiative Decay Counter (RDC)

Photons contributing to accidental background come from either RMD, bremsstrahlung, or positron AIF. The AIF background decreases in MEG II with respect to MEG thanks to the reduced mass of the CDCH compared to the MEG drift chambers. The yield of the AIF background photons above 48 MeV per muon decay expected from MC simulations is

1.4×10^{-6} , to be compared with 2.3×10^{-6} in MEG. On the other hand the RMD photon background does not change. The RDC, an additional detector newly installed in MEG II, is capable of identifying a fraction of low-energy positrons from RMD decays with photon energies close to the kinematic limit.

The detector consists of 12 plastic scintillators BC-418 for time measurement and 76 LYSO crystals for energy measurement. It is placed 140 cm downstream of the muon stopping target and covers the region within 10 cm from the beam axis. It identifies low-energy positrons (1–5 MeV) in time coincidence with the detection of a high energy photon in the LXe detector. According to simulations, it can detect about $\sim 40\%$ of RMD background with $E_\gamma > 48$ MeV improving the sensitivity of the $\mu^+ \rightarrow e^+ \gamma$ search by $\sim 10\%$.

If we place another module of RDC upstream of the target, we can identify the other half of the RMD positrons emitted towards the upstream side. However, the upstream RDC is technically challenging because it must be placed in the beam path. Several detector techniques have been examined; currently the best candidate is a resistive plate chamber with extremely low-mass diamond-like carbon based electrodes. Though the upstream RDC is not included in the baseline design of MEG II at this moment, intensive R&D work is underway.

2.5. The Trigger and Data Acquisition System

The MEG II sensitivity goal required a substantial re-design of the readout electronics to deal with a factor of two increase in muon stopping rate with respect to MEG and an almost tripling in the number of electronic channels. Since the physical space for the electronics could not be expanded, the only option was to combine the previous DAQ, trigger and high-voltage systems into a combined single system. The result is the new WaveDAQ system [25], consisting of four distinguished subsystems. First, the system is housed in a full custom crate with integrated remote controlled power supply (24 V / 360 W) and a custom backplane featuring gigabit serial links in a dual star topology. The second system is the WaveDREAM (Drs4 based REAdout Module) board (WDB), which on one hand digitizes all input signals with a sampling frequency up to 5 GSPS / 12 bit and on the other hand performs continuous trigger operations at 80 MHz such as summing all input channels and comparing the result to a predefined threshold. In addition, the WDB can house a high voltage generator for SiPM biasing. The third system is a dedicated Trigger Concentrator Board (TCB), which receives all digital trigger data from one crate, combines and processes them, then sends the result to a central trigger system also consisting of the same board type, where the final global trigger decision is made every 12.5 ns. The fourth system is the Data Concentrator Board (DCB), which receives the DAQ data stream from each WDB and sends it to the central computer via Gigabit Ethernet lines.

3. Results

In this section the results of the engineering runs carried out in the years 2017–2020 are reported.

During the engineering runs, the muon beam was delivered at different intensities, up to the MEG II nominal intensity ($7 \times 10^7 \mu^+/\text{s}$) and stopped in the target. Beam tuning and measurements were performed taking advantage of the new beam monitoring tools, which allowed continuous measurement of the beam conditions. The scintillating fibre and matrix detectors were frequently used during the runs, providing the beam profile and rate consistent with those measured by the pill and APD counter at the beginning of the runs. The target camera system has been extensively tested and showed the capability to detect target displacements at the required precision level (100 μm for movements along the direction transverse to the target plane). In 2020, a π^-p charge-exchange run was performed, in which the beam was changed from positive muons to 70.5 MeV/ c negative pions and the muon

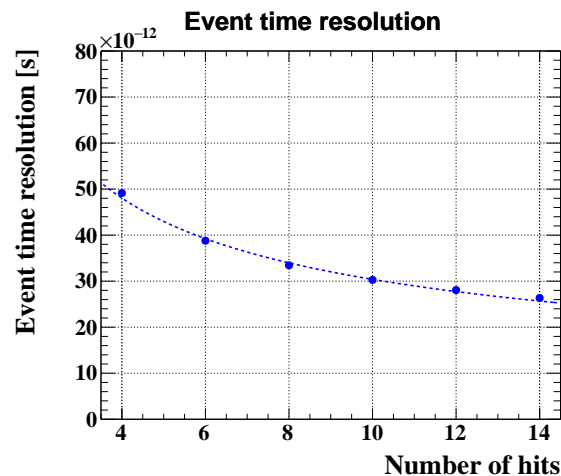


Figure 2. The pTC time resolution as function of the number of hit counters from the 2017 engineering run.

stopping target was replaced with a liquid hydrogen target to induce the reaction $\pi^- p \rightarrow \pi^0 n$. Photons from the subsequent decay $\pi^0 \rightarrow \gamma\gamma$ are used for LXe calibration purposes.

The DAQ and the trigger system operated successfully enabling stable data taking during the runs. A limited number of DAQ channels was available because the mass production of the full electronics was not yet started, awaiting the detailed results from the prototype test. Various problems were identified and solved; in particular common noise was reduced to a level that does not affect the photon energy resolution. The trigger was successfully commissioned and performed well during the runs. The full system has been deployed in spring 2021 with about 9,000 channels reading out the whole MEG II detectors. A first test showed that the system can run at an event rate of 50 Hz resulting in a data stream of about 8 GBit/s.

The pTC was the first sub-detector which was fully commissioned already during the first engineering run, in 2017. It operated in the nominal MEG II muon beam. The background e^+ hit rate was confirmed to be less than 100 kHz as expected. Radiation damage to SiPMs was carefully studied. The dark current in the SiPMs gradually increases during the use of the beam while the impact on the time resolution is kept under control by cooling the detector to 10 °C. The e^+ time is reconstructed by combining hit times after subtracting the time-of-flight between counters. It is expected to be calculated from the e^+ trajectory given by the CDCH but the highly segmented design of pTC allows the tracking of e^+ using the hit pattern. This pTC-alone tracking was used to evaluate the pTC time resolution; Figure 2 shows the resolution measured with the 2017 data as a function of the number of hits. The measured resolution is worse than the expectation from the tests with a ^{90}Sr source made before the installation because of the larger noise level in the MEG II environment. By weighting with the distribution of the number of the hits for the signal e^+ s obtained by a Monte Carlo (MC) simulation and correcting for a bias in the evaluation method, the overall time resolution is estimated to be 35 ps, a factor of two better than that in MEG (76 ps). After three years of physics run, the resolution is expected to deteriorate to 41 ps due to the radiation damage, still satisfying the requirement of about 40 ps. In the 2018–2020 runs, only one sector, either upstream or downstream, was installed to provide a trigger to the DAQ for taking Michel e^+ data together with the CDCH.

The CDCH has been integrated into the experiment since 2018. Due to the limited DAQ channels available during the engineering runs a complete particle tracking test was not possible. Nonetheless, the chamber was tested with cosmic rays and different beam intensities

up to the MEG II nominal one; tests with different gas mixtures were also performed. A few wire breaks, due to corrosion that started before the chamber was put in an inert atmosphere, occurred during the runs, requiring electrical insulation of part of the chamber to continue data-taking. The broken wires had to be removed at the end of the beam periods after re-opening the detector. Anomalous high currents (up to 300 μA) were observed in parts of the CDCH during the runs, that were cured after optimizing the gas mixture and operating the chamber with up to 2% oxygen. As a result, the chamber was operated in stable conditions at the full MEG II beam intensity with He/isobutane (90/10) + isopropyl alcohol (1%) + O_2 (0.5%) for a period of about one week during 2020 run. Front-end (FE) electronics with three different amplifications were used to investigate the optimum electronics gain value. The total gain (gas gain \times FE gain) was measured using cosmic ray data by comparing amplitude and charge spectra to MC simulations which contain a detailed description of ionization patterns, drift and diffusion from Garfield, single electron pulse shapes from prototype measurements under UV laser light as well as the noise spectra measured on data. The configuration with the highest FE gain has been chosen and is currently under implementation (a modification of all the FE board is required) since it has been demonstrated that it provides the best signal to noise ratio. A direct measurement of the gas gain was also extracted from the currents of the HV power supplies, taking into account the hit rate that could be also directly measured from data. Measurements of the gain are in the range of $4 - 7 \times 10^5$ in the mixture He/isobutane 90/10 plus 1% isopropyl alcohol. Studies with simulations and data have been carried out to understand the impact of oxygen in order to optimize the gas mixture. We do not expect a significant deterioration of the chamber performances caused by the use of oxygen concentrations at the level 0.5% or below considering also the expected improvements deriving from the larger signal to noise ratio of the modified electronics.

The limited number of hits on reconstructed tracks, due to the small number of readout channels, does not allow an accurate measurement of the spatial resolution and of the CDCH performances. Thus, the expected performances of the fully instrumented detector have been evaluated by MC simulations, updated with noise, gain and electronics response observed in data. Positron efficiency and angular resolution are currently worse than the design (65% and 6.7 mrad vs. 70% and about 5 mrad, respectively), the vertex resolutions are already at the design level (about 1.7 mm and 0.8 mm along the beam and vertical directions, respectively) while the momentum resolution is better than the design (100 keV/c vs. 130 keV/c). The efficiency loss is due to the higher than expected noise levels. We observe both low-frequency coherent noise over sets of wires on the same WaveDREAM board as well as incoherent noise extending to higher frequencies. Digital filters have been developed to cope with it, but an intensive campaign for the identification and suppression of hardware noise sources is foreseen for the 2021 engineering run. The improved momentum resolution is due to an improved track fitting method for tracks with multiple turns in the chamber.

The upgraded LXe detector was put into operation in 2017 and calibrated with sources, LED, low-energy photons from a nuclear reaction using a Cockcroft–Walton accelerator [26] and finally with high-energy photons in the 2020 π^-p charge-exchange run. The RMD and background spectra were acquired with the muon beam at different intensities. The long-term stability of the PMTs and MPPCs was investigated and a degradation of the photosensor performance was observed under muon beam conditions. A PMT gain decrease at the MEG II nominal intensity was first observed to be faster than the expected based on the MEG experience in 2018, but the deterioration speed moderated year by year. We decided to halve the gain to further mitigate the gain decrease and the current gain decrease rate measured in 2020 (0.16%/day) is now consistent with the expectation, which enables the PMTs to operate over the full MEG II data taking period.

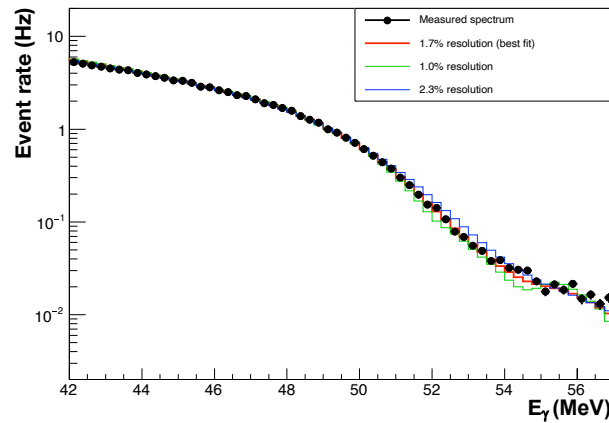


Figure 3. A measured background photon spectrum in the 2019 run at the MEG II beam intensity (black points) as well as MC simulation spectra convoluted with different energy resolution assumptions. The red histogram shows 1.7% resolution case (best fit), and green/blue show 1.0%/2.3%, respectively.

The MPPC VUV light sensitivity (PDE) was measured to be 12% in the experiment, lower than that measured in laboratory tests, which was $>15\%$. Moreover, the PDE further decreased during the runs. In the 2020 run, the deterioration speed was lower than in 2019 (0.03 %/hour instead of 0.06 %/hour, where 0.03 %/hour means that the PDE will go to zero in $100/(0.03\%/hour)$, about 139 days.). Possible causes considered are the hole trapping at the sensor surface induced by VUV light or irradiation at low temperature. A possible solution was identified by annealing at high temperatures which removes accumulated charges. The effect was demonstrated with several MPPCs in the LXe detector; the PDEs recovered to values $>15\%$. The optimum annealing strategy for all MPPCs is currently under investigation. Since the timing resolution would be dominated by PMT timing resolution in the case of the small MPPC PDE, MC simulations showed that almost no degradation of the MEG II sensitivity occurs down to 5% PDE, which is good enough to guarantee the sensitivity reach. If the degradation is saturated at this value, annealing may not be necessary.

A preliminary estimate of the detector performance was made. The position resolution was measured using photons from the ${}^7\text{Li}(p,\gamma){}^8\text{Be}$ reaction excited using the Cockcroft–Walton proton accelerator with a 5 mm wide slit collimator. Improvements in both horizontal and vertical resolution were observed (about 2.5 mm), twice better than MEG. The energy resolution was evaluated by fitting background photon spectra from muon decays using the MC distributions as shown in Figure 3 and from monochromatic 55 MeV photons from the π^-p charge-exchange reaction, which provide consistent results of 1.7% in the signal region. The improved granularity of the photon incident face almost eliminates the depth dependence of the energy resolution. The resolution seems at the level of the worst case scenario considered in [13]; however the data analysis is still preliminary and the results are evaluated using a limited number of electronics channels. The intrinsic time resolution, which was estimated by the difference of times reconstructed by even and odd channels, is 39 ps, consistent with the MC expectation.

The downstream RDC successfully demonstrated the RMD detection capability under muon beam conditions during the engineering runs, by observing positrons in time coincidence with high energy photons in LXe. The peak in Figure 4 represents coincident hits by a γ and a positron from RMD. The fraction of events at the time coincident peak is found to be consistent with the expectation from simulation. An upstream RDC prototype based on resistive plate chambers with diamond-like-carbon based electrodes is being developed and

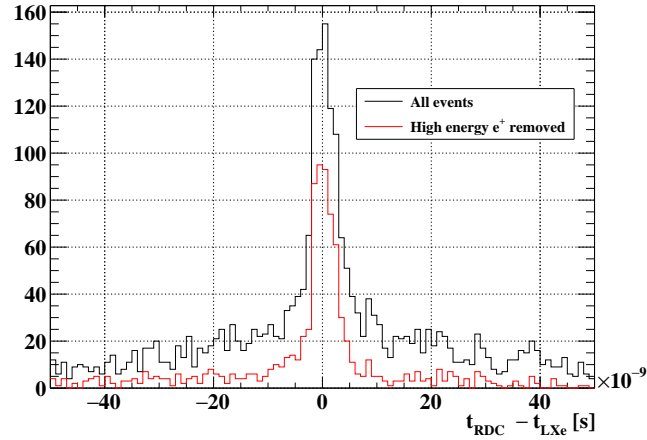


Figure 4. Distribution of time differences between RDC and LXe detectors for the events triggered by a high energy γ at the LXe detector (black). The peak corresponds to the RMD events. The flat time distribution corresponds to accidental hits of high energy positrons from Michel decays, which is reduced by applying an energy cut ($E_{e^+}^{\text{LYSO}} < 8$ MeV, red histogram).

showed a good efficiency and time resolution in laboratory. The first tests under muon beam conditions were performed during the 2020 run.

4. Discussion

All the detector components were integrated into the MEG II experiment and tested in the engineering runs, which enables us to identify and solve issues prior to the start of physics data collection. Based on the results from the engineering runs, we re-evaluated the projected sensitivity of MEG II. We input the updated detector performance, listed in Table 1 (MEG II updated), to the sensitivity calculation; however, note that some of the parameters were evaluated on more realistic MC simulations, updated on the basis of observation on data, and others on the data but the results are still preliminary. The following is assumed here:

- The DAQ time is 20 weeks per year with 84% live time for three years;
- The muon stopping rate is $7 \times 10^7 \mu^+/\text{s}$;
- The PDE of VUV-MPPCs is at a constant value of 6%;
- The upstream RDC is not included.

The *sensitivity* is defined as the median of 90% confidence branching-ratio upper limits for the background-only hypothesis. In three years, we will reach a sensitivity of 6×10^{-14} , which is roughly one order of magnitude better than MEG's sensitivity of 5.3×10^{-13} . The expected single event sensitivity is 1×10^{-14} . In the realistic evaluation of the detector performance, some parameters improved while others became worse than the assumed design parameters; however the overall projected sensitivity stays almost the same as that reported in Ref. [13]. The data statistics is 5.6 times larger than MEG, and the remaining improvement of a factor 1.6 comes from lower background due to the improved detector resolutions. Actually, the sensitivity improvement is not yet saturated and an extension of DAQ time can improve the sensitivity reach further.

If the degradation of VUV-MPPC PDE is not saturated at a value above 5%, we have to recover it by the annealing process. Because annealing all the MPPCs takes a couple of months, it can be done only during the annual accelerator shutdown period. In this case, the obtainable statistics is limited by the accumulated beam intensity up to which the MPPC is operational. For the given statistics, it is better to run for the full beam time at a reduced beam

Table 1. Summary of detector performance. Two values for σ_{E_γ} are values for shallow (<2 cm) / deep (>2 cm) events.

	$\sigma_{p_{e^+}}$	$\sigma_{\theta_{e^+}}$	σ_{E_γ}	σ_{x_γ}	$\sigma_{t_{e^+\gamma}}$	ϵ_{e^+}	ϵ_γ
MEG	380 keV/c	9.4 mrad	2.4%/1.7%	5 mm	122 ps	30%	63%
MEG II design	130 keV/c	5.3 mrad	1.1%/1.0%	2.4 mm	84 ps	70%	69%
MEG II updated	100 keV/c	6.7 mrad	1.7%/1.7%	2.4 mm	70 ps	65%	69%

intensity since the number of accidental background events has a quadratic dependence on the beam intensity. Moreover, the detector performance is better with a lower beam intensity due to a low pileup probability. For example, the positron reconstruction efficiency improves from 65% at $7 \times 10^7 \mu^+/\text{s}$ to 74% at $3.5 \times 10^7 \mu^+/\text{s}$ with the current reconstruction algorithms. As a result, it was shown by a preliminary study that a comparable sensitivity is achievable at a stopping rate down to $3.5 \times 10^7 \mu^+/\text{s}$, with which the VUV-MPPCs can operate for 20 weeks of DAQ based on the degradation speed observed in the engineering runs.

Cathode and field wires of the CDCH suffer from corrosion caused by exposure to humidity during construction. The risk of possible wire breakings during data taking imposed the construction of a new backup chamber with different cathode and field wires. The new chamber will use more robust 50 μm diameter Ag-coated aluminum wires, instead of the old 40 μm ones, for which the final drawing process, which was verified to weaken the wires and make them more prone to corrosion, will be avoided. Construction of the new chamber will take approximately 18 months; in the meanwhile the existing one will be used in the experiment.

At the time of writing, preparation for the 2021 engineering run is underway. In this run, all the detector signals will be collected for the first time with the full readout electronics. The stability and performance of the existing CDCH and the long-term behaviour of the PDE degradation of the VUV-MPPCs will be extensively studied. We plan to collect data with a $\mu^+ \rightarrow e^+ \gamma$ trigger at the end of the run, which will be the first physics data of MEG II.

Funding: This research was funded by DOE DEFG02-91ER40679 (USA), INFN, MIUR Montalcini D.M. 2014 n. 975 (Italy), JSPS Core-to-Core Program, A. Advanced Research Networks JPJSCCA20180004, JSPS KAKENHI Grant Numbers JP26000004, JP18K13557, JP19J13635, JP19J21535, JP19J21730, JP20H00154, JP21H00065 (Japan), the Russian Federation Ministry of Science and Higher Education (Russia), and Schweizerischer Nationalfonds (SNF) Grant 200020_172706 and Grant 206021_177038 (Switzerland).

Acknowledgments: We are grateful for the support and co-operation provided by PSI as the host laboratory and to the technical and engineering staff of our institutes.

Conflicts of Interest: The authors declare no conflict of interest.

References

1. Calibbi, L.; Signorelli, G. Charged Lepton Flavor Violation: an experimental and theoretical introduction. *Riv. Nuovo Cimento* **2018**, *41*, 71–174, [arXiv:hep-ph/1709.00294]. doi:10.1393/ncr/i2018-10144-0.
2. Abi, B.; Albahri, T.; Al-Kilani, S. et al. Measurement of the Positive Muon Anomalous Magnetic Moment to 0.46 ppm. *Phys. Rev. Lett.* **2021**, *126*, 141801. doi:10.1103/PhysRevLett.126.141801.
3. Calibbi, L.; López-Ibañez, M.L.; Melis, A. et al. Implications of the Muon g-2 result on the flavour structure of the lepton mass matrix, 2021, [arXiv:hep-ph/2104.03296].
4. Baldini, A.M.; Bao, Y.; Baracchini, E. et al. (MEG Collaboration). Search for the lepton flavour violating decay $\mu^+ \rightarrow e^+ \gamma$ with the full dataset of the MEG experiment. *Eur. Phys. J. C* **2016**, *76*, 434, [arXiv:hep-ex/1605.05081]. doi:10.1140/epjc/s10052-016-4271-x.
5. Kinsho, M.; Ikegami, M.; Kawamura, N. et al. Proposal of an Experimental Search for $\mu^- \rightarrow e^-$ Conversion in Nuclear Field at Sensitivity of 10^{-14} with Pulsed Proton Beam from RCS. https://j-parc.jp/researcher/Hadron/en/pac_1101/pdf/KEK_J-PARC-PAC2010-13.pdf, 2010.

6. Abramishvili, R.; Adamov, G.; Akhmetshin, R.R. et al. (COMET Collaboration). COMET Phase-I Technical Design Report. *Prog. Theor. Exp. Phys.* **2020**, 2020, 033C01. doi:10.1093/ptep/ptz125.
7. Bertl, W.; Engfer, R.; Hermes, E. et al. (SINDRUM II Collaboration). A search for $\mu^- \rightarrow e^-$ conversion in muonic gold. *Eur. Phys. J. C* **2006**, 47, 337–346. doi:10.1140/epjc/s2006-02582-x.
8. Abrams, R.; Alezander, D.; Ambrosio, G. et al. (Mu2e Collaboration). Mu2e Conceptual Design Report, 2012, [arXiv:physics.ins-det/1211.7019].
9. Arndt, K.; Augustin, H.; Baesso, P. et al. Technical design of the phase I Mu3e experiment, 2021, [arXiv:physics.ins-det/2009.11690].
10. Bellgardt, U.; Otter, G.; Eichler, R. et al. Search for the decay $\mu^+ \rightarrow e^+e^+e^-$. *Nucl. Phys. B* **1988**, 299, 1–6. doi:10.1016/0550-3213(88)90462-2.
11. Kou, E.; Urquijo, P.; Altmannshofer, W. et al. The Belle II Physics Book. *Prog. Theor. Exp. Phys.* **2019**, 2019, 123C01. doi:10.1093/ptep/ptz106.
12. Hao, Z.; Ren-You, Z.; Liang, H. et al. Searching for $\tau \rightarrow \mu\gamma$ lepton-flavor-violating decay at super Charm-Tau factory. *Eur. Phys. J. C* **2016**, 76, 421, [arXiv:hep-ph/1602.01181]. doi:10.1140/epjc/s10052-016-4251-1.
13. Baldini, A.M.; Baracchini, E.; Bemporad, C. et al. (MEG II Collaboration). The design of the MEG II experiment. *Eur. Phys. J. C* **2018**, 78, 380. doi:10.1140/epjc/s10052-018-5845-6.
14. Adam, J.; Bai, X.; Baldini, A.M. et al. The MEG detector for $\mu^+ \rightarrow e^+\gamma$ decay search. *Eur. Phys. J. C* **2013**, 73, 2365, [arXiv:physics.ins-det/1303.2348]. doi:10.1140/epjc/s10052-013-2365-2.
15. Palo, D.; Hildebrandt, M.; Hofer, A. et al. Precise Photographic Monitoring of MEG II Thin-film Muon Stopping Target Position and Shape. *Nucl. Instrum. Methods A* **2019**, 944, 162511. doi:10.1016/j.nima.2019.162511.
16. Cavoto, G.; Chiarello, G.; Hildebrandt, M. et al. A photogrammetric method for target monitoring inside the MEG II detector. *Rev. Sci. Instrum.* **2021**, 92, 043707. doi:10.1063/5.0034842.
17. Baldini, A.M. et al. Single-hit resolution measurement with MEG II drift chamber prototypes. *J. Instrum.* **2016**, 11, P07011, [arXiv:physics.ins-det/1605.07970]. doi:10.1088/1748-0221/11/07/P07011.
18. Garfield++ – simulation of gaseous detectors. <https://garfieldpp.web.cern.ch/garfieldpp/>.
19. Ansys® Electronic Desktop 2019.
20. ISEG EHS 8630p-305F. <http://www.iseg-hv.com>.
21. Baldini, A.M.; Baracchini, E.; Cavoto, G. et al. Gas Distribution and Monitoring for the Drift Chamber of the MEG-II Experiment. *J. Instrum.* **2018**, 13, P06018, [arXiv:physics.ins-det/1804.08482]. doi:10.1088/1748-0221/13/06/P06018.
22. Boca, G.; Cattaneo, P.W.; De Gerone, M. et al. Timing resolution of a plastic scintillator counter read out by radiation damaged SiPMs connected in series. *Nucl. Instrum. Methods A* **2021**, 999, 165173, [arXiv:physics.ins-det/2005.05027]. doi:10.1016/j.nima.2021.165173.
23. Boca, G.; Cattaneo, P.W.; De Gerone, M. et al. The laser-based time calibration system for the MEG II pixelated Timing Counter. *Nucl. Instrum. Methods A* **2019**, 947, 162672, [arXiv:physics.ins-det/1907.00911]. doi:10.1016/j.nima.2019.162672.
24. Ieki, K.; Iwamoto, T.; Kaneko, D. et al. Large-area MPPC with enhanced VUV sensitivity for liquid xenon scintillation detector. *Nucl. Instrum. Methods A* **2019**, 925, 148–155. doi:10.1016/j.nima.2019.02.010.
25. Galli, L.; Baldini, A.M.; Cei, F. et al. WaveDAQ: An highly integrated trigger and data acquisition system. *Nucl. Instrum. Methods A* **2019**, 936, 399–400. doi:10.1016/j.nima.2018.07.067.
26. Adam, J.; Bai, X.; Baldini, A. et al. (MEG Collaboration). Calibration and monitoring of the MEG experiment by a proton beam from a Cockcroft–Walton accelerator. *Nucl. Instrum. Methods A* **2011**, 641, 19–32. doi:10.1016/j.nima.2011.03.048.